International Journal of Mechanical Sciences 53 (2011) 262–270

Contents lists available at ScienceDirect

International Journal of Mechanical Sciences

journal homepage: www.elsevier.com/locate/ijmecsci

Calculation of forming limit diagrams using Hill's 1993 yield criterion

A. Rezaee-Bazzaz [a], H. Noori [b], R. Mahmudi [c,*]

[a] Department of Metallurgy and Materials Engineering, Faculty of Engineering, Ferdowsi University of Mashhad, Mashhad, Iran
[b] Department of Mechanical Engineering, McMaster University, Hamilton, Ont., Canada L8S 4L7
[c] School of Metallurgical and Materials Engineering, University of Tehran, Tehran, Iran

ARTICLE INFO

Article history:
Received 2 September 2009
Received in revised form
14 January 2011
Accepted 20 January 2011
Available online 28 January 2011

Keywords:
Forming limit diagram
Yield criterion
Strain hardening
Strain rate sensitivity

ABSTRACT

Based on the analysis proposed by Jones and Gillis (JG), forming limit diagrams (FLDs) are calculated from idealization of sheet deformation into three stages: (I) homogeneous deformation up to maximum load, (II) deformation localization under constant load, and (III) local necking with precipitous drop in load. In the calculation, Hill's 1993 yield criterion is used. Using this yield criterion and the JG model, effects of materials parameters such as ratio of uniaxial to equi-biaxial yield stress, strain hardening, strain rate sensitivity and plastic anisotropy on the shape and level of forming limit curves are studied. In addition, the capability of the JG model to predict limit strains is demonstrated through comparison of calculated results with experimental data for the interstitial free (IF) steel and aluminum alloys 3003-O and 8014-O. It is concluded that although the model predicts the effect of material parameters reasonably well, the calculated limit strains are higher than the experimental FLDs. The observed discrepancy may be attributed to the assumption of planar isotropy, cavitation and the nature of texture present in the sheets. Due to the overestimation of the predictions, care must be taken when using this approach for industrial purposes.

1. Introduction

Forming Limit Diagrams (FLDs), first proposed by Keeler [1] and Goodwin [2] are generally used as a diagnostic tool for sheet metal formability over various loading paths. They show the limit strains the material can sustain in different modes of deformation, including drawing and stretching states. While the experimental construction of the FLD is well established in the literatures [1–4], many attempts have been made to numerically calculate the FLDs, which might be less time consuming in die design and trouble-shooting processes. The main concept in the modeling sheet metal response in different processes is how the material yields and fails in a specific condition. Based on sheet metal properties and process parameters, different approaches have been used for the explanation of necking phenomenon and the calculation of FLDs. The method used by Marciniak and Kuczynski [5] may be the most prevalent model which is considered in this field of study. In their model, the assumption of the existence of an initial imperfection as a groove in the sheet plane and its behavior compared with the adjacent regions in the material is considered for the simulation of what happens in reality. Many researchers have tried to apply this model in conjunction with different yield criteria and hardening laws. The results show the dependency of the calculation on the used yield criteria, constitutive equations, as well as the initial size of the assumed imperfection in the material [6–10]. There have been some attempts to consider the effect of cavitation and void growth in prediction of FLDs. Kim and Kim [11] incorporated the void growth concept in the M–K method to predict the forming limit diagram of steel sheets. They used the Avrami-like equation for relating density changes due to void growth and strain during stage II but they could not find reasonable results and found that the best coincidence between analysis and experiment was obtained by assuming an unrealistic value of the inhomogeneity factor or Avrami-like parameters. Date and Padmanabhan [12] used the same approach for considering the effect of cavitation on prediction of the FLD of steel, Al–Mg, Al–Cu–Mg and Al–Mn sheets. They found a good correlation between the experimentally determined and predicted FLDs of steel by combining M–K theory with Hutchinson–Tvergaard equation for all strain ratios, or using the same equation for negative strain ratios. They concluded that satisfactory predictions could be obtained once the deformation and fracture behavior of a material are known. There are clear evidences showing that the assumption of an imperfection for occurrence of failure in sheet metals is not necessary and therefore, analyzing limit strains that are independent of such a presumption would be valuable. This point of view was initiated by Gillis and Jones [13] who proposed their theory

* Corresponding author. Tel.: +98 21 8208 4137; fax: +98 21 8800 6076.
E-mail address: mahmudi@ut.ac.ir (R. Mahmudi).

0020-7403/$ - see front matter © 2011 Elsevier Ltd. All rights reserved.
doi:10.1016/j.ijmecsci.2011.01.007

based on modeling of the easily observable features from a tensile test of a typical sheet metal. According to this model, plastic deformation is approximated by three phases as schematically shown in Fig. 1:

Phase (I) homogeneous deformation up to maximum load (point *H*);

Phase (II) deformation localization under constant load (up to point *J*); and

Phase (III) local necking with a precipitous drop in load.

These three phases are not exactly the same as what happens in reality. They are idealization of physical processes into certain mathematical assumptions which can be used with material behavior approximations and boundary conditions to derive solvable equations for modeling sheet behavior during various stages of deformation.

The capability of this analysis to predict FLDs have been discussed in some papers. Jones and Gillis [14,15] and Choi et al. [16,17] applied the JG model using a generalized anisotropic yield criterion for calculation of FLDs. Later, Pishbin and Gillis [18] used Hill's non-quadratic flow law (case IV) for sheets having planar isotropy to calculate the FLDs of AK steel and various aluminum alloy sheets. Aghaie et al. [19,20] applied Hosford criterion as a special case of Hill's non-quadratic flow law in the prediction of the FLDs for aluminum sheets obeying the power law and Voce constitutive equations. More recently, Noori and Mahmudi [21] compared the ability of the JG model to calculate FLDs using three different yield criteria of Hill's 1948, Hill's 1979, and Hosford's 1979 using a constant cross-head speed deformation program. These yield criteria have different approaches to the anisotropy phenomenon. Based on their work, it was found that the accuracy of predictions depends on the measured mechanical properties of the material, the applied yield criterion, and the method of strain measurement which determines how experimental FLDs are passed through the measured strain points.

In the present work, Hill's 1993 criterion in conjunction with the JG analysis is used for predicting FLDs. This third order criterion employs both equi-biaxial and uniaxial yield stresses. It is expected that it improves the numerical method in metal forming simulation and yields more accurate results than those predicted by the other Hill's criteria.

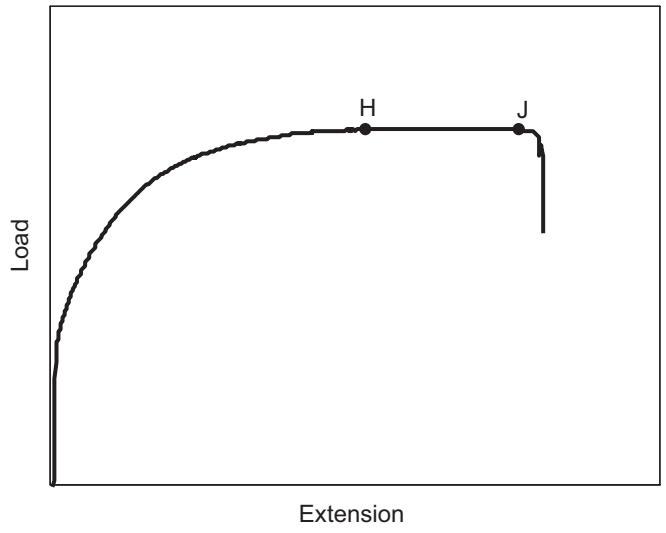

Fig. 1. Schematic representation of the three deformation phases. Points *H* and *J* are, respectively, denoted as the end of homogeneous deformation (phase I) and the deformation under constant load (phase II).

2. General description

Hill's 1993 yield criterion [22] has been used in this study to calculate the stress components from the strain and strain rate components. This yield criterion can be written as

$$\frac{\sigma_1^2}{\sigma_0^2}-\frac{c\sigma_1\sigma_2}{\sigma_0\sigma_{90}}+\frac{\sigma_2^2}{\sigma_{90}^2}+\left\{(p+q)-\frac{(p\sigma_1+q\sigma_2)}{\sigma_b}\right\}\frac{\sigma_1\sigma_2}{\sigma_0\sigma_{90}}=1 \tag{1}$$

where p and q may be obtained from the following relationships:

$$\left(\frac{1}{\sigma_0}+\frac{1}{\sigma_{90}}-\frac{1}{\sigma_b}\right)p=\frac{2r_0(\sigma_b-\sigma_{90})}{(1+r_0)\sigma_0^2}-\frac{2r_{90}\sigma_b}{(1+r_{90})\sigma_{90}^2}+\frac{c}{\sigma_0} \tag{2}$$

$$\left(\frac{1}{\sigma_0}+\frac{1}{\sigma_{90}}-\frac{1}{\sigma_b}\right)q=\frac{2r_{90}(\sigma_b-\sigma_{90})}{(1+r_{90})\sigma_{90}^2}-\frac{2r_0\sigma_b}{(1+r_0)\sigma_0^2}+\frac{c}{\sigma_0} \tag{3}$$

where c is given by

$$\frac{c}{\sigma_0\sigma_{90}}=\frac{1}{{\sigma_0}^2}+\frac{1}{{\sigma_{90}}^2}-\frac{1}{{\sigma_b}^2} \tag{4}$$

In the above equations, σ_1 and σ_2 are the principal stress components in the sheet plane. σ_0 and σ_{90} are defined as uniaxial initial yield stresses in the respective rolling and transverse directions, r_0 and r_{90} are the corresponding normal plastic anisotropy parameters and σ_b is initial yield stress under equi-biaxial tension.

For sheets having planar isotropy, assuming that $\sigma_0=\sigma_{90}=\overline{\sigma}$, where $\overline{\sigma}$ is the uniaxial tension yield stress, and $r_0=r_{90}=r$, where r is the normal plastic anisotropy parameter, the yield criterion proposed by Hill may be written in the following form:

$$\sigma_1^2-\left(2-\frac{\overline{\sigma}^2}{\sigma_b^2}\right)\sigma_1\sigma_2+{\sigma_2}^2+\left\{(p+q)-\frac{(p\sigma_1+q\sigma_2)}{\sigma_b}\right\}\sigma_1\sigma_2=\overline{\sigma}^2 \tag{5}$$

Using the associated flow rules for plastic deformation, each strain rate component can be found as a function of stress components in the following form:

$$\dot{\varepsilon}_1=\dot{\lambda}\left[2\sigma_1-\left(2-p-q-\frac{\overline{\sigma}^2}{\sigma_b^2}\right)\sigma_2-\frac{q}{\sigma_b}\sigma_2^2-\frac{2p}{\sigma_b}\sigma_1\sigma_2\right] \tag{6}$$

$$\dot{\varepsilon}_2=\dot{\lambda}\left[2\sigma_2-\left(2+p+q-\frac{\overline{\sigma}^2}{\sigma_b^2}\right)\sigma_1-\frac{p}{\sigma_b}\sigma_1^2-\frac{2q}{\sigma_b}\sigma_1\sigma_2\right] \tag{7}$$

The geometry of the element of sheet undergoing plastic deformation with a neck formed is introduced in Fig. 2. Following the JG analysis, the initial length, width, and thickness of the test specimen are denoted by L_0, w_0, and $2h_0$, respectively. These

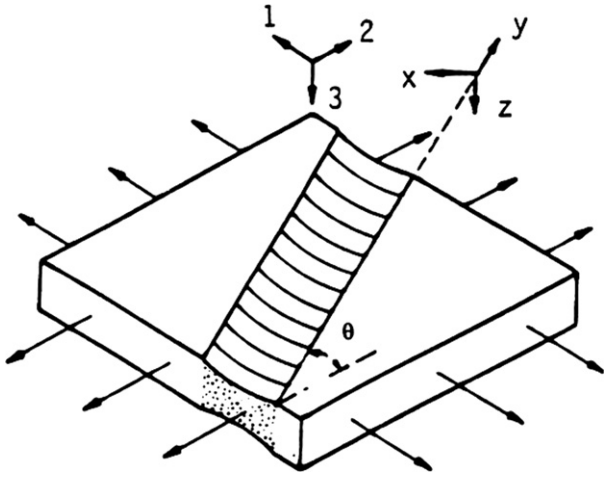

Fig. 2. The geometry of neck formation in the sheet. The localized neck is inclined at an angle θ to the 2-axis when strain rate ratio is negative.

dimensions after plane stress deformation are denoted by L, w, and $2h$ in such a way that $L > L_0$. Length and width dimensions are in the 1 and 2 directions, respectively. Throughout the test, it is assumed that the principal axes of deformation coincide with these dimensions of the test element.

Fig. 2 shows the neck coordinate system x, y, and z. The y-axis is along the direction of neck formation; the z-axis coincides with the thickness direction; and the x-axis is perpendicular to both y and z. If the minimum thickness in the deforming sheet, the sheet thickness at the critical cross section, is denoted by $2a$, the logarithmic principal strains at this minimum cross section are defined as

$$\varepsilon_3 = \ln\left(\frac{a}{h_0}\right) \tag{8}$$

$$\varepsilon_2 = \ln\left(\frac{w}{w_0}\right) \tag{9}$$

$$\varepsilon_1 = -(\varepsilon_2 + \varepsilon_3) = \ln\left(\frac{h_0 w_0}{aw}\right) \tag{10}$$

In order to perform the calculations, a deformation program must be specified. In the present case, constant average strain rates in the length and width directions are assumed during the initial homogenous phase of the process. For cases involving biaxial stretching, right hand side (RHS) of the FLD, constancy of logarithmic strain rate in the width direction continues throughout the deformation process. For the cases involving negative minor strains in the left hand side (LHS) of the FLD, however, as neck formation proceeds, the width strain rate is assumed to be proportional to the strain rate in length direction. Thus, for the RHS and LHS during phase I:

$$\frac{\dot{L}}{L} = \alpha = \text{constant} \tag{11}$$

$$\frac{\dot{w}}{w} = \beta = \text{constant} \tag{12}$$

The above equations are also applicable during phases II and III in the RHS of FLD. For the LHS, during phases II and III:

$$\frac{\dot{L}}{L} = \alpha \tag{13}$$

$$\dot{\varepsilon}_2 = \left(\frac{\beta}{\alpha}\right)\dot{\varepsilon}_1, \quad \beta \le 0 \tag{14}$$

Here as neck formation proceeds, the longitudinal strain rate varies along the length and so does the width strain rate. For a given material, α is held constant and β varies over a set of discrete cases from uniaxial tension through plane strain to equi-biaxial stretching. For uniaxial tension, $\beta/\alpha = -r/(1+r)$; for plane stain tension, $\beta = 0$; and for equi-biaxial stretching, $\beta = \alpha$.

Based on Hill's velocity discontinuity analysis [23] of the localized necking description in thin sheets under plane stress state, the localized plastic deformation is believed to have zero rate of extension. This will be true for deformation with the negative strain rate ratio ($\dot{\varepsilon}_2/\dot{\varepsilon}_1$) that leads to neck formation at the nonzero angle θ between w and neck direction. This angle will be zero for $\dot{\varepsilon}_2 = 0$ to satisfy Hill's assumption. Although this condition for neck formation cannot be applied when $\dot{\varepsilon}_2 > 0$, it is assumed that neck direction is the same as that in-plane strain state ($\dot{\varepsilon}_2 = 0$), which is perpendicular to the length direction.

3. Plasticity relationships

Introducing the variable X as the ratio of the in-plane stresses ($X = \sigma_2/\sigma_1$) and t as the ratio of the largest principal stress to the equi-biaxial yield stress ($t = \sigma_1/\sigma_b$), Eq. (5) can be written as

$$\sigma_1^2[1-(2-{a_1}^2)X + X^2 + (p+q)X - ptX - qtX^2] = \overline{\sigma}^2 \tag{15}$$

where $a_1 = \overline{\sigma}/\sigma_b$.

In deriving Eq. (15), it has been considered that $\sigma_2/\sigma_b = tX$, which can be obtained from the definition of t and X by some simple mathematical calculations. Rearranging Eq. (15) gives the following equation:

$$\frac{\sigma_1}{\overline{\sigma}} = \{1-(2-a_1^2)X + X^2 + (p+q)X - ptX - qtX^2\}^{-1/2} \tag{16}$$

Using Eqs. (6) and (7), $\rho = \dot{\varepsilon}_2/\dot{\varepsilon}_1$ can be expressed as

$$\rho = \frac{2X - (2+p+q-a_1^2) - pt - 2qtX}{2-(2-p-q-a_1^2)X - qtX^2 - 2ptX} \tag{17}$$

Applying the energy equilibrium:

$$\overline{\sigma}\dot{\overline{\varepsilon}} = \sigma_1\dot{\varepsilon}_1 + \sigma_2\dot{\varepsilon}_2 \tag{18}$$

The effective stain rate can be formulated as

$$\dot{\overline{\varepsilon}} = \frac{1}{(\overline{\sigma}/\sigma_1)}(1+X\rho)\dot{\varepsilon}_1 \tag{19}$$

4. Phase I deformation

During phase I, homogenous deformation is assumed and therefore, the critical cross section is indistinguishable from all other cross sections. The criterion for maximum load in direction 1 is described by Considere criterion [24]:

$$\frac{\dot{\sigma}_1}{\sigma_1} = \dot{\varepsilon}_1 \tag{20}$$

When this condition is satisfied, phase I terminates. This point is called H, as shown in Fig. 1. The assumption of an initial homogenous phase leads to

$$\begin{aligned} \dot{\varepsilon}_1 &= \alpha \\ \dot{\varepsilon}_2 &= \beta \end{aligned} \tag{21}$$

5. Phase II deformation

After reaching the maximum load, point H, deformation will gradually localize, leading to the formation of a distinct neck. Physically, phase II is characterized by a gradual concentration of deformation into the vicinity of some critical cross sections that are less hardened than the other cross sections in the sheet. These critical cross sections may be actually softer than other sections of the sheet, and/or geometrical imperfections such as specimen preparation defects, and/or metallurgical imperfections like inclusions, precipitates, and segregations in these sections may cause reduction of the strength. For the purpose of analyzing this phase, the assumption of homogenous deformation is replaced with the assumption that the load in direction 1 remains constant and thus, Eq. (20) not only characterizes the onset of phase II but also remains valid throughout this phase at the critical cross section. The assumption of load constancy has experimentally been verified for the IF steel sheets, as reported by Chamanfar and Mahmudi [25].

In the LHS of FLD, the in-plane strain rate ratio, ρ, is assumed to be constant for any strain path. Therefore, considering Eq. (17), the in-plane stress ratio, X, and ratio of the largest principal stress to equi-biaxial yield stress, t, are assumed to be constant. Hence, according to Eq. (16), $\overline{\sigma}/\sigma_1$ is constant. Let the value of this constant be c_1; inserting ρ, X, and c_1 into Eq. (19), results in

$$\dot{\overline{\varepsilon}} = \frac{1}{c_1}(1+X\rho)\dot{\varepsilon}_1 \tag{22}$$

Similarly, letting $1/c_1(1+X\rho)$ equal to c_0:

$$\dot{\bar{\varepsilon}} = c_0 \dot{\varepsilon}_1 \tag{23}$$

Moreover, as explained above:

$$\bar{\sigma} = c_1 \sigma_1 \tag{24}$$

Inserting Eq. (24) into Eq. (20) results in

$$\frac{\dot{\bar{\sigma}}}{\bar{\sigma}} = \frac{\dot{\sigma}_1}{\sigma_1} = \dot{\varepsilon}_1 \tag{25}$$

Considering the power law hardening:

$$\bar{\sigma} = k' \bar{\varepsilon}^n \dot{\bar{\varepsilon}}^m \tag{26}$$

Thus

$$\frac{\dot{\bar{\sigma}}}{\bar{\sigma}} = \frac{n}{\bar{\varepsilon}} \dot{\bar{\varepsilon}} + \frac{m}{\dot{\bar{\varepsilon}}} \ddot{\bar{\varepsilon}} \tag{27}$$

By some mathematical calculations, it can be shown that

$$\bar{\varepsilon} = c_0 \varepsilon_1 \tag{28}$$

$$\ddot{\bar{\varepsilon}} = c_0 \ddot{\varepsilon}_1 \tag{29}$$

where $\ddot{\bar{\varepsilon}}$ is the second time derivative of equivalent strain. Combining Eqs. (23), (27), (28) and (29), the following relationship is obtained:

$$\frac{n}{\varepsilon_1} \dot{\varepsilon}_1 + \frac{m}{\dot{\varepsilon}_1} \ddot{\varepsilon}_1 = \dot{\varepsilon}_1 \tag{30}$$

or

$$\ddot{\varepsilon}_1 = \left(1 - \frac{n}{\varepsilon_1}\right) \frac{\dot{\varepsilon}_1^{\,2}}{m} \tag{31}$$

This is the governing differential equation during phase II for the LHS of FLD which is equivalent to that calculated by Pishbin and Gillis [16] for the LHS of FLD using Hill's non-quadratic yield criterion.

In the positive minor strain region of FLD, $\dot{\varepsilon}_2$ is assumed to remain uniform throughout the sheet. In this case, $\dot{\bar{\varepsilon}}$ is no longer simply proportional to $\dot{\varepsilon}_1$. Considering Eq. (19) and knowing that $\rho\dot{\varepsilon}_1 = \beta$, the following equation is obtained:

$$\dot{\bar{\varepsilon}} = \frac{1}{(\bar{\sigma}/\sigma_1)} (\dot{\varepsilon}_1 + X\beta) \tag{32}$$

Considering the definition of t and a_1, the relationship between σ_1 and $\bar{\sigma}$ is as follows:

$$\sigma_1 = \frac{t}{a_1} \bar{\sigma} \tag{33}$$

Therefore,

$$\frac{\dot{\sigma}_1}{\sigma_1} = \frac{\dot{\bar{\sigma}}}{\bar{\sigma}} + \frac{\dot{t}}{t} \tag{34}$$

As mentioned earlier, considering power law hardening, when load in direction 1 remains constant:

$$\frac{n}{\bar{\varepsilon}} \dot{\bar{\varepsilon}} + \frac{m}{\dot{\bar{\varepsilon}}} \ddot{\bar{\varepsilon}} + \frac{\dot{t}}{t} = \dot{\varepsilon}_1 \tag{35}$$

Combining Eqs. (32), (33) and (35), the following equation is obtained:

$$\frac{\dot{t}}{t} + \frac{n\dot{\bar{\varepsilon}}}{\bar{\varepsilon}} + \frac{m\dot{t}}{t} + m \frac{\ddot{\varepsilon}_1 + \dot{X}\beta}{\dot{\varepsilon}_1 + X\beta} = \dot{\varepsilon}_1 \tag{36}$$

Using Eq. (17) and knowing that in the RHS of FLD, $\dot{\varepsilon}_2 = \beta$, the following equation for $\dot{\varepsilon}_1$ is obtained:

$$\dot{\varepsilon}_1 = \beta \left(\frac{2 - (2 - p - q - a_1^2)X - qtX^2 - 2ptX}{2X - (2 + p + q - a_1^2) - pt - 2qtX} \right) \tag{37}$$

Considering Eq. (37), we will have

$$\ddot{\varepsilon}_1 = \beta \left[\frac{(-(2-p-q-a_1^2)\dot{X} - q\dot{t}X^2 - 2qtX\dot{X} - 2p\dot{t}X - 2pt\dot{X})\eta - (2\dot{X} - p\dot{t} - 2q\dot{t}X - 2qt\dot{X})\zeta}{\eta^2} \right] \tag{38}$$

where

$$\eta = 2X - (2 + p + q - a_1^{\,2}) - pt - 2qtX \tag{39}$$

$$\zeta = 2 - (2 - p - q - a_1^{\,2})X - qtX^2 - 2ptX \tag{40}$$

Combining Eqs. (36) and (38) and after some mathematical calculations we will have:

$$n\frac{\dot{\bar{\varepsilon}}}{\bar{\varepsilon}} + \dot{t}\left[\frac{1+m}{t} + \frac{(-qX^2 - 2pX)\eta - (-p - 2qX)\zeta}{\eta^2} \cdot \frac{m\beta}{\dot{\varepsilon}_1 + X\beta}\right] + \dot{X}\left\{\frac{m\beta}{\dot{\varepsilon}_1 + X\beta} + \frac{-[-(2-p-q-a_1^{\,2}) - 2qtx - 2pt]\eta - (2 - 2qt)\zeta}{\eta^2} \frac{m\beta}{\dot{\varepsilon}_1 + X\beta}\right\} = \dot{\varepsilon}_1 \tag{41}$$

On the other hand, the yield function can be written in the following form:

$$\left[aq\left(\frac{t}{a_1}\right)^3 - \left(\frac{t}{a_1}\right)^2\right]X^2 + \left[ap\left(\frac{t}{a_1}\right)^3 - (p + q - 2 + a_1^{\,2})\left(\frac{t}{a_1}\right)^2\right]X + \left[1 - \left(\frac{t}{a_1}\right)^2\right] = 0 \tag{42}$$

Finding X as a function of t, the following equations are obtained:

$$X = \frac{-[ap(t/a_1)^3 - (p + q - 2 + a_1^{\,2})(t/a_1)^2] + \sqrt{\Delta}}{2[aq(t/a_1)^3 - (t/a_1)^2]} \tag{43a}$$

or

$$X = \frac{-[ap(t/a_1)^3 - (p + q - 2 + a_1^{\,2})(t/a_1)^2] - \sqrt{\Delta}}{2[aq(t/a_1)^3 - (t/a_1)^2]} \tag{43b}$$

where Δ is obtained from the following equation:

$$\Delta = \left[ap\left(\frac{t}{a_1}\right)^3 - (p + q - 2 + a_1^{\,2})\left(\frac{t}{a_1}\right)^2\right] - 4\left[aq\left(\frac{t}{a_1}\right)^3 - \left(\frac{t}{a_1}\right)^2\right]\left[1 - \left(\frac{t}{a_1}\right)^2\right] \tag{43c}$$

Only one of the above equations is admissible; because there should exist only one relationship between X and t. Bearing in mind that the relationship between X and t should be valid for all values of X and t in the loading region; the values of X and t at point H should satisfy the equation and from this fact, the admissible equation can be chosen.

The procedure of finding values of X and t at point H is as follows:

Using Eq. (15), the definition of ρ, and considering that the Hill's 1993 yield function, after some mathematical calculations, the following equation is obtained:

$$D = \frac{\sigma_1}{\bar{\sigma}} = \frac{2(\rho - X) + (p + q - 2 + a_1^2)(\rho X - 1)}{[(2p + qX)X\rho - (p + 2qX)]a_1} \tag{44}$$

Combining Eqs. (42) and (44) and knowing that $t/a_1 = \sigma_1/\bar{\sigma}$, the following equation is obtained:

$$(a_1 pX + a_1 qX^2)D^3 - [1 + X^2 + (p + q - 2 + a_1^2)X]D^2 + 1 = 0 \tag{45}$$

Eq. (45) involves two variables X and ρ. Once the strain rate ratio, ρ, is given, the stress ratio, X can be solved for, and then D is determined using Eq. (44) from which t can be calculated. The range of ρ is within 0 and 1; however, Eq. (45) is a highly non-linear equation. There may exist more than one solution

for a given value of ρ. In order to find the correct solution, the following steps are used [26]:

1. Solving Eq. (45) and finding all solutions for X.
2. Eliminating solutions corresponding to complex and negative values of X as well as those solutions which are greater than 1.
3. Eliminating solutions corresponding to negative values of D.
4. For the rest of solutions, ρ is subjected to a small positive perturbation, $\Delta\rho$. Solving Eq. (45) again and comparing $(D)_{\rho+\Delta\rho}$ with $(D)_\rho$. If $(D)_{\rho+\Delta\rho}<(D)_\rho$, then X is the correct solution for the given value of ρ.

Differentiating Eq. (42) respect to time and rearranging the resultant equation leads to the following expression:

$$\dot{X}=\frac{(2t/{a_1}^2)[1+X^2+(p+q-2+{a_1}^2)X]-(3t^2/{a_1}^3)(a_1pX+a_1qX^2)}{(a_1p+2a_1qX)(t/a_1)^3-(2X+p+q-2+{a_1}^2)(t/a_1)^2}\dot{t} \tag{46}$$

Substituting Eq. (46) into Eq. (41) and after some mathematical simplification, the following equation is obtained:

$$\dot{t}=\left(\dot{\varepsilon}_1-\frac{n\dot{\bar{\varepsilon}}}{\bar{\varepsilon}}\right)\div\Lambda \tag{47}$$

where

$$\Lambda=\left[\frac{1+m}{t}+\frac{m\beta}{\eta^2(\dot{\varepsilon}_1+X\beta)}\left[(-qX^2-2pX)\eta-(-p-2qX)\zeta\right]+\left(\frac{m\beta}{\eta^2(\dot{\varepsilon}_1+X\beta)}\Gamma+\frac{m\beta}{\dot{\varepsilon}_1+X\beta}\right)\xi\right] \tag{48}$$

and

$$\Gamma=[-(2-p-q-a_1^2)-2qtX-2pt]\eta-(2-2qt)\zeta \tag{49}$$

$$\xi=\frac{(2t/a_1^2)[1+X^2+(p+q-2+a_1^2)X]-3t^2/a_1^3(a_1pX+a_1qX^2)}{(a_1p+2a_1qX)(t/a_1)^3-(2X+p+q-2+a_1^2)(t/a_1)^2} \tag{50}$$

$\dot{\bar{\varepsilon}}$, ε_1 and t can be obtained, solving the system of differential equations including Eqs. (32), (37) and (47).

It is noteworthy that solving the system of differential equations requires expressing X as a function of t, using one of Eqs. (43a) or (43b). The initial values of ε_1 and $\bar{\varepsilon}$ are n and c_0n, respectively, and the initial value of t is obtained by finding the value of X at point H following the procedure mentioned before.

6. Phase III deformation

Physically, deformation mode of this phase is identified by necking under rapidly decreasing load rather than localizing under nearly constant load. This behavior is caused by the formation of a well-developed neck centered at the critical section. For analysis phase III of deformation, a description of the neck shape is needed. Based on the previous analyses, for example Noori and Mahmudi [21], the neck is assumed to have some shape that has been described by Bridgman [27]. This neck is assumed to obey the kinematic constraint given by

$$d/R=k\ln(h_0/d) \tag{51}$$

where R is the radius of the curvature of the trace of the neck, $2d$ is the minimum thickness in the deforming sheet and k is a constant taken here as 3/4.

The analysis considers the deformation rate for the 1 direction of the sheet to find thinning rate, $\dot{\varepsilon}_n$, at the minimum cross section. In order to accommodate the prescribed deformation program in the 1 direction by the strain only within the neck, the material velocity component normal to the neck must be considered. Hill's velocity discontinuity analysis can be used to derive the necessary formulation [23]. The thinning rate in the minimum cross section during phase III is:for the LHS

$$\dot{\varepsilon}_n=\frac{(1+\rho)(L_0/(2h_0))(\dot{L}/L_0)\cos\theta\, k\varepsilon_n^2\exp\{\varepsilon_n\}}{F(\varepsilon_n)} \tag{52}$$

for the RHS

$$\dot{\varepsilon}_n=\frac{(L_0/(2h_0))(\dot{L}/L_0)k\varepsilon_n^2\exp\{\varepsilon_n\}+\varepsilon_n\dot{\varepsilon}_2\sin\Phi}{F(\varepsilon_n)} \tag{53}$$

where

$$F(\varepsilon_n)\equiv 2[(1+2\varepsilon_n+k\varepsilon_n^2)^2/(1+2+(k\varepsilon_n))]^{1/2}\times\arctan[\varepsilon_n(2+k\varepsilon_n)/(2+2\varepsilon_n+k\varepsilon_n^2)]^{1/2}-(1+\varepsilon_n+k\varepsilon_n^2)\Phi \tag{54}$$

and Φ and θ are given by

$$\cos\Phi=(1+\varepsilon_n)/(1+\varepsilon_n+k\varepsilon_n^2) \tag{55}$$

$$\theta=\frac{1}{2}\arccos[(1+\rho)/(1-\rho)] \tag{56}$$

The specific procedure for deriving the above equations has been given by Pishbin and Gliss [18]. After developing the equations for determining phase III thinning rate as a function of ε_n, it is necessary to relate the neck strain, ε_n, to condition in phase II as follows:

$$\varepsilon_n=-\varepsilon_3(\mathrm{II})+\ln\left[\frac{1+2\varepsilon_n+k\varepsilon_n^2}{1+\varepsilon_n+k\varepsilon_n^2}\right] \tag{57}$$

The above equation can be solved numerically by successive approximation or using an appropriate computer subroutine such as the "*fzero*" function in MATLAB software. Once the value of ε_n is obtained from Eq. (57), it is substituted into Eq. (52) or (53), depending on the LHS or the RHS of FLD to be predicted, to calculate the thinning rate. After determining the thinning rate in the minimum cross section, the strain rate is easily obtained as

$$\dot{\varepsilon}_1(\mathrm{III})=\dot{\varepsilon}_n/(1+\rho)\quad\text{for the LHS of the FLD} \tag{58}$$

$$\dot{\varepsilon}_1(\mathrm{III})=\dot{\varepsilon}_n-\dot{\varepsilon}_2\quad\text{for the RHS of the FLD} \tag{59}$$

Consequently, the transition from phase II to phase III occurs when $\dot{\varepsilon}_1(\mathrm{II})=\dot{\varepsilon}_1(\mathrm{III})$, and this point, J, can be located numerically in a straightforward manner [18]. This procedure is repeated using suitably small integration steps until phase II terminates with the onset of phase III, localized necking.

7. Determination of the limit strains

When point J is located, theoretical FLD can be plotted by determining the limit strains. It is noted that the final strains in the immediate vicinity of the failure are not measured experimentally for constructing the FLDs. Actual limit strains are mainly measured at some distance away from the failure [4]. In the present analysis, it is assumed that once the neck forms, the minor strain at point J, ε_2^J, remains constant throughout phase III. Therefore, ε_2^J can be used to determine the limit strains near the edge of the neck as follows [18]:

$$\varepsilon_1^*=-\varepsilon_2^J-\varepsilon_3(\mathrm{II}) \tag{60}$$

$$\varepsilon_2^*=\varepsilon_2^J \tag{61}$$

where ε_1^* and ε_2^* are limit strains and ε_2^J is obtained by the following equations for the LHS and RHS of FLD, respectively:

$$\varepsilon_2^J=\rho\varepsilon_n/(1+\rho)\quad\text{for the LHS of the FLD} \tag{62}$$

$$\varepsilon_2^J=\varepsilon_2(\mathrm{II})\quad\text{for the RHS of the FLD} \tag{63}$$

Table 1
Mechanical properties of the studied materials.

Material	Angle to the rolling direction (deg.)	Strain hardening exponent (n)	Strain rate sensitivity index (m)	Plastic strain ratio (r)	ratio of uniaxial to equi-biaxial yield stress (a_1)
IF steel	0	0.26	0.008	2.05	0.87[a]
	45	0.25[b]	0.008[b]	1.94[b]	
	90	0.25	0.009	2.41	
3003-O aluminum	0	0.190	–	1.08	
	45	0.200[c]	0.005[d]	0.85[c]	0.97[e]
	90	0.193	–	0.25	
8014-O aluminum	0	0.240	0.009[f]	0.540	
	45	0.200[f]	–	0.800[f]	0.92[f]
	90	0.220	–	0.420	

[a] Ref. [7].
[b] Ref. [21].
[c] Ref. [28].
[d] Ref. [16].
[e] Ref. [29].
[f] Ref. [30].

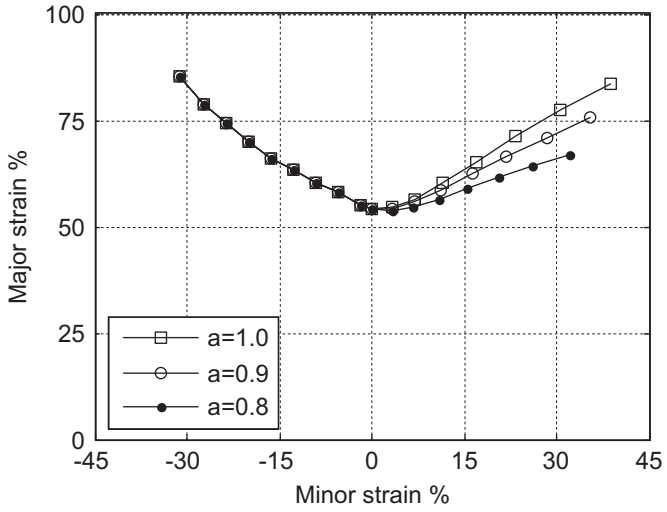

Fig. 3. Influence of a_1 on the calculated FLD for IF steel.

The obtained values of the limit strains are transformed to engineering strain values to plot the FLD.

8. Results and discussion

In order to check the results of the present analysis, comparisons were made with experimental FLDs. All the materials' constants needed for the calculation of FLDs, taken from other works [7,16,21,28–30], are given in Table 1. In the calculation of FLDs, average of weighted values of orientation-dependent mechanical properties, such as n and r defined as $x=(x_0+2x_{45}+x_{90})/4$, are used.

8.1. Influence of a_1 on the prediction of the FLDs

The effect of a_1-value on the calculated FLDs is demonstrated in Fig. 3. It can be seen that decreasing the difference between uniaxial and biaxial initial yield stresses increases the limit strains in the RHS of FLD but has no effect on the LHS of FLD. Since our calculation method for the LHS of FLD, including plane strain point, is independent of the employed yield function, it is expected that variation in a_1-value does not affect the limit strain in this region. This independence has already been shown to be valid as our derivations leading to Eq. (31) do not include any term depending on the yield function. However, the increased level of FLD in the RHS could be related to the effect of a_1-value on the yield surface shape. Fig. 4 shows that the yield surface shape will be much more rounded with increasing a_1-value. It is concluded that a less stretched initial yield surface in the biaxial tension region results in much more limit strains. This is in agreement with the view of Barlat [31] working on the texture and anisotropic yield surface of sheet metals.

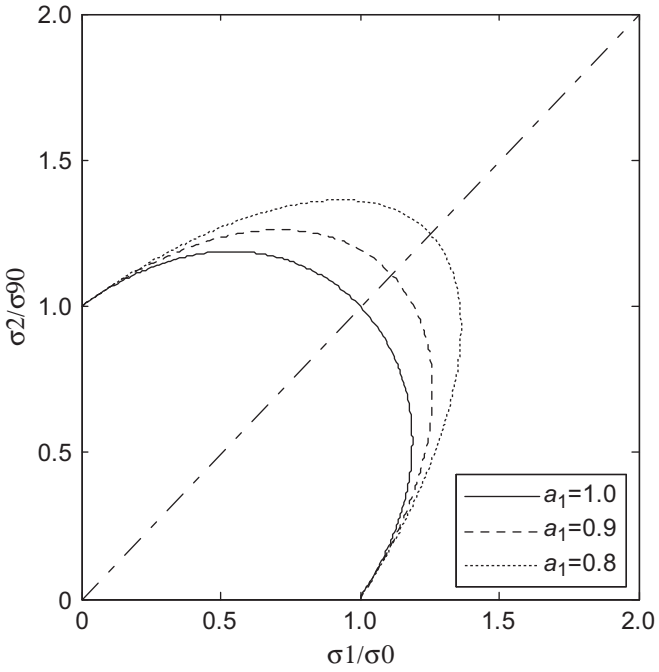

Fig. 4. Influence of a_1 on the yield surface ($n=0.25$, $m=0.008$ and $r_0=r_{90}=r=2.09$).

8.2. Influence of materials' parameters

Different parameters affect the forming limits of sheet metals in stamping processes. They can be viewed as material and process parameters, the influences of which have been investigated in the literatures [31–36]. Strain hardening, strain rate sensitivity, and plastic anisotropy are the important parameters

which are considered in the present prediction methodology. Interstitial free steel is taken as a representative material, the data of which are used in the prediction program. In the computations, when one parameter changes, all the others are kept constant. Fig. 5 shows the effect of strain hardening exponent (n) on the calculated FLDs for the IF sheet steel with $a_1=0.87$, $m=0.008$, and $r=2.09$. It can be seen that increasing the value of n from 0.15 to 0.25 results in raising the level of both sides of FLD. This is in agreement with the experimental observations indicating that better strain distribution is achieved by higher strain hardening exponent.

In Fig. 6, the effect the of strain rate sensitivity parameter (m) on FLD is demonstrated. Similar to the n value, changing m-values from 0.005 to 0.009 while keeping $a_1=0.87$, $n=0.25$ and $r=2.09$ shifts up the predicted limit strains. It should be noted, however, that materials' parameters such as n and m are not necessarily uncoupled and in reality, it is not always possible to keep one constant while changing the other. It is well known that rate insensitive materials have a plane strain forming limit of about n. Rate sensitivity can raise limit strain through material strengthening in the diffuse and local necks and therefore allowing the material outside the necks to be deformed more. It means that the major limit strain exceeds the value n with higher m-values.

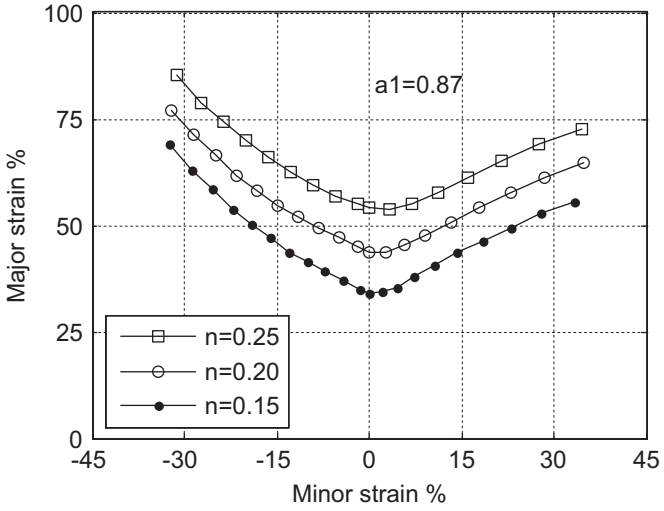

Fig. 5. Influence of strain hardening exponent (n) on the calculated FLD for IF steel ($m=0.008$, $r=2.09$).

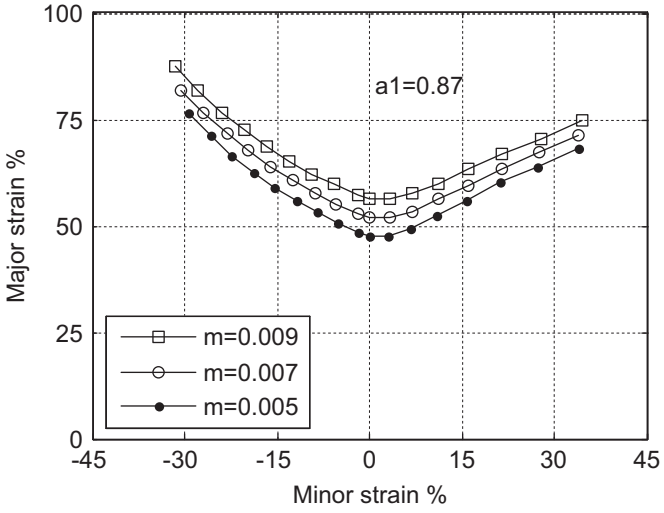

Fig. 6. Influence of strain-rate sensitivity parameter (m) on the calculated FLD for IF steel ($n=0.25$, $r=2.09$).

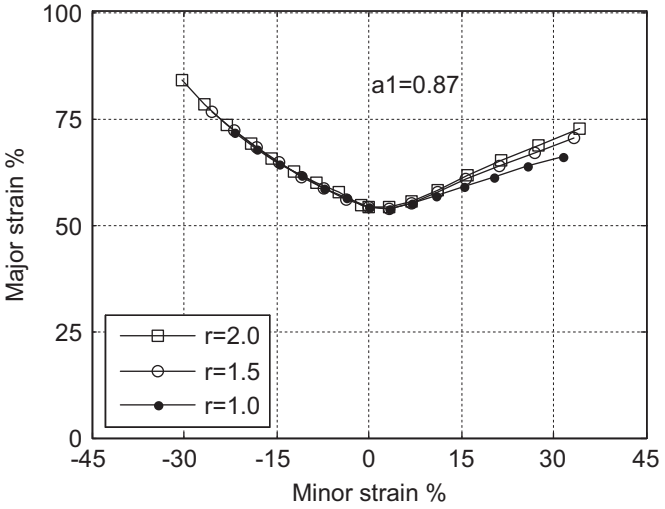

Fig. 7. Influence of plastic anisotropy parameter (r) on the calculated FLD for IF steel ($n=0.25$, $m=0.008$).

Fig. 7 shows the influence of plastic anisotropy parameter (r) on the calculated FLD for $a_1=0.87$, $n=0.25$ and $m=0.008$ obtained for the IF sheets. The FLD is predicted at three different r-values. It is observed that increasing the value of the average plastic anisotropy parameter increases the level of FLD in the RHS region. This might be explained by means of the variation of initial yield surface shape with changing plastic anisotropy parameter. Similar to what is explained for the effect of a_1-value on the predicted FLD, it could be mentioned that much more rounded initial yield surface shape in the stretching region eventuates at the higher level of FLD for positive minor strain region of FLD. In the LHS of FLD, increasing r-value increases the range of limit strains, although no significant change is observed in the level of FLDs. Although it has been reported [31] that the experimental FLDs are independent of plastic anisotropy parameter, the numerical results obtained in this study show that the calculated limit strains are sensitive to the changes in r-value.

8.3. Comparison with experiments

The capability of the model to predict experimental results is investigated through the comparison of the calculated FLD with three materials forming limit curves including IF steel, aluminum 3003-O, and aluminum 8014-O. The experimental data for mechanical properties of these materials are reported in the literature. As shown in Figs. 8–10, all of the predicted FLDs are overestimated. However, the best prediction in the shape of FLD belongs to aluminum 8014-O. The observed discrepancies might have been caused by the employed constitutive equations, judgment of the neck, and neck strain measurement, as well as the FLD construction methodology. Furthermore, the assumption of planar isotropy, cavitation and the nature of texture present in the sheets might have all contributed to the observed differences. It is also worthy to be noted that the material properties such as n and m have been extracted from uniaxial tensile test. These properties have been used for other strain paths such as plane strain and equi-biaxial tension stress states. It is expected to obtain closer predictions if the material parameters for different

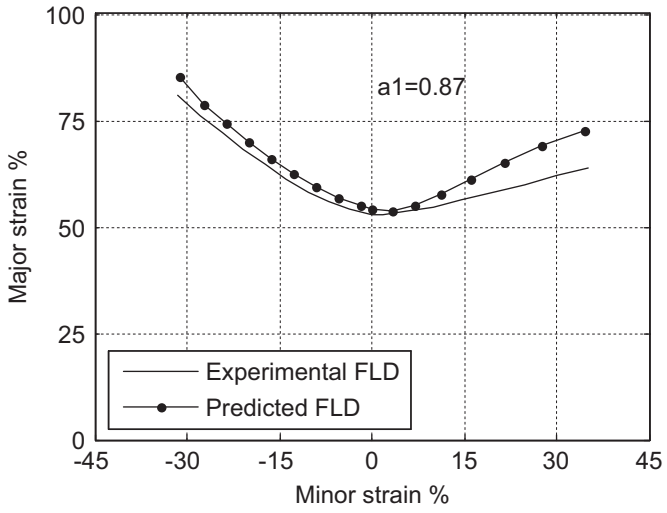

Fig. 8. Experimental and predicted FLDs for IF steel. Experimental data are from [21].

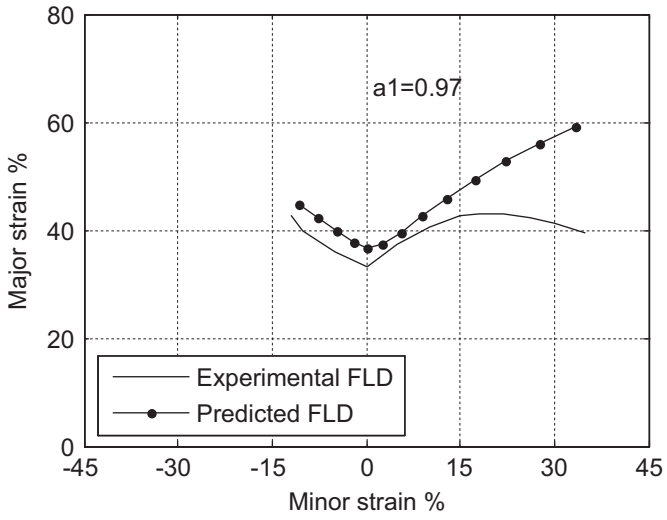

Fig. 9. Experimental and predicted FLDs for Aluminum 3003-O. Experimental data are from [28].

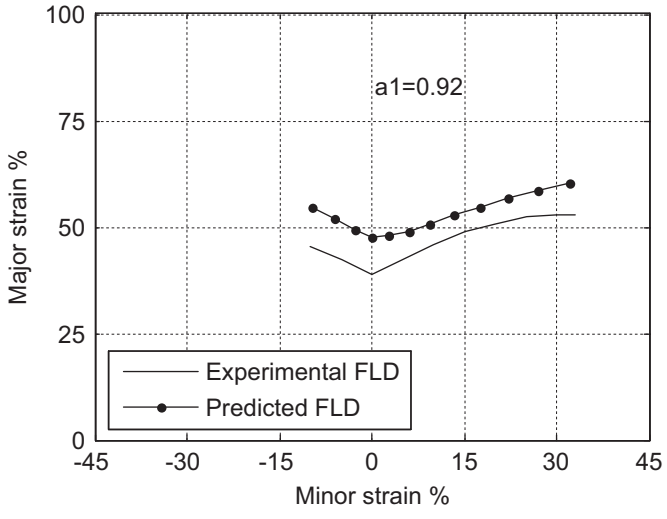

Fig. 10. Experimental and predicted FLDs for Aluminum 8014-O. Experimental data are from [30].

strain paths were used instead of those obtained in uniaxial tension. This may result in a better shape of both LHS and RHS of the predicted FLDs.

9. Conclusions

An analytical method is presented for calculating FLDs of sheet materials. It is based on three phase deformation idealization of Jones and Gillis and uses the Hill's 1993 user friendly yield criterion. The model is capable of predicting the forming limit strains achievable during sheet metal forming operations for rate sensitive sheets having planar isotropy which obeys the power law constitutive equation. The material parameters needed for the calculation are: the strain hardening parameter (n), the strain rate sensitivity factor (m), the average plastic anisotropy ratio (r), and the ratio of uniaxial yield stress to equi-biaxial one (a_1). The model consists of two computer programs; one for negative strain region and the other for the positive strain region of FLD. Homogeneous straining in the minor strain direction throughout all three phases of deformation in the prediction of RHS of FLD and proportional straining in the prediction of the LHS of FLD have been assumed. The calculated FLDs using the present analysis show the expected trends of increasing the limit strains as the strain rate sensitivity parameter (m), or the strain hardening exponent (n) increase. Near equi-biaxial stretching, the forming limit strains increase with an increase in a_1 but this parameter has no effect on the LHS limits. An increase in the plastic anisotropy ratio (r) increases limit strains on the RHS of FLD and does not change the level of limit strain on the LHS but increases the extent of FLD. The observed discrepancy between the theoretical and the experimental FLDs, may be attributed to the assumption of planar isotropy, cavitation and the nature of texture present in the sheets.

References

[1] Keeler SP. Determination of the forming limits in automobile stamping. Sheet Met Ind 1965;42:683–91.
[2] Goodwin GM. Application of strain analysis to sheet-metal-forming problems in the press shop. Metall Ital 1968;60:767–74.
[3] Ghosh AK, Hecker SS. Stretching limits in sheet metals: in-plane versus out-of-plane deformation. Metall Trans 1974;5:2161–4.
[4] Hecker SS. Simple technique for determining forming limit curves. Sheet Metal Ind 1975;52:671–6.
[5] Marciniak Z, Kuczynski K. Limit strains in the processes of stretch-forming sheet metal. Int J Mech Sci 1967;9:609–12.
[6] Allwood JM, Shouler DR. Generalised forming limit diagrams showing increased forming limits with non-planar stress states. Int J Plasticity 2009;25:1207–30.
[7] Aretz H. Numerical analysis of diffuse and localized necking in orthotropic sheet metals. Int J Plasticity 2007;23:798–840.
[8] Cao J, Yao H, Karafillis A, Boyce MC. Prediction of localized thinning in sheet metal using a general anisotropic yield criterion. Int J Plasticity 2000;16:1105–29.
[9] Hiwatashi S, Van Bael A, Van Houtte P, Teodosiu C. Prediction of forming limit strains under strain-path changes: application of an anisotropic model based on texture and dislocation structure. Int J Plasticity 1998;14:647–69.
[10] Vegter H, Van den Boogaard AH. A plane stress yield function for anisotropic sheet material by interpolation of biaxial stress states. Int. J. Plasticity 2006;22:557–80.
[11] Kim KH, Kim DW. The effect of void growth on the limit strain of steel sheets. Int J Mech Sci 1983;25:293–300.
[12] Date PP, Padmanabhan KA. On the prediction of the forming limit diagram of sheet metals. Int J Mech Sci 1992;34:363–74.
[13] Gillis PP, Jones SE. Tensile deformation of a flat sheet. Int J Mech Sci 1979;21:109–17.
[14] Jones SE, Gillis PP. Analysis of biaxial stretching of a flat sheet. Metall Trans A 1984;15:133–8.
[15] Jones SE, Gillis PP. Generalized quadratic flow law for sheet metals. Metall Trans A 1984;15:129–32.
[16] Choi W, Gillis PP, Jones SE. Calculation of the forming limit diagram. Metall Trans A 1989;20:1975–87.

[17] Choi W, Gillis PP, Jones SE. Forming limit diagrams. In: Wagoner RH, Chan KS, Keeler SP, editors. Forming limit diagrams: concepts, methods and applications. PA: TMS Warendale; 1989. p. 215–37.
[18] Pishbin H, Gillis PP. Forming limit diagrams calculated using Hill's nonquadratic yield criterion. Metall Trans A 1992;23:2817–31.
[19] Aghaie-Khafri M, Mahmudi R. Predicting of plastic instability and forming limit diagrams. Int J Mech Sci 2004;46:1289–306.
[20] Aghaie-Khafri M, Mahmudi R, Pishbin H. Role of yield criteria and hardening laws in the prediction of forming limit diagrams. Metall Trans A 2002;33:1363–71.
[21] Noori H, Mahmudi R. Prediction of forming limit diagrams in sheet metals using different yield criteria. Metall Trans A 2007;38:2040–52.
[22] Hill R. A user-friendly theory of orthotropic plasticity in sheet metals. Int J Mech Sci 1993;35:19–25.
[23] Hill R. On discontinuous plastic states, with special reference to localized necking in thin sheets. J Mech Phys Solids 1952;1:19–30.
[24] Considere A. Ann Ponts Chausses 1885;9:574–775.
[25] Chamanfar A, Mahmudi R. Effect of specimen geometry, gage length, and width measurement locations on plastic strain ratio (*R*-value) in sheet metals. Metall Trans A 2006;37:3477–87.
[26] Xu S, Weinmann KJ. Prediction of forming limit curves of sheet metals using Hill's 1993 user-friendly yield criterion of anisotropic materials. Int J Mech Sci 1998;40:913–25.
[27] Bridgman PW. Studies in large plastic flow and fracture. New York, NY: Mc Graw-Hill; 1952. p. 26.
[28] Hecker SS. Formability of aluminum alloy sheets. J Eng Mater Technol, Trans ASME 1975;97H:66–73.
[29] Hu W. Constitutive modeling of orthotropic sheet metals by presenting hardening-induced anisotropy. Int J Plasticity 2007;23:620–39.
[30] Mahmudi R. Forming limits in biaxial stretching of aluminum sheets and foils. J Mater Proc Technol 1993;37:203–16.
[31] Barlat F. Crystallographic texture, anisotropic yield surfaces and forming limits of sheet metals. Mater Sci Eng. 1987;91:55–72.
[32] Hosford WF, Duncan JL. Sheet metal forming: a review. JOM 1999;51: 39–44.
[33] Lee D, Zaverl Jr. F. Neck growth and forming limits in sheet metals. Int J Mech Sci 1982;24:157–73.
[34] Marciniak Z, Duncan JL, Hu SJ. Mechanics of sheet metal forming. 2nd ed. Oxford: Butterwort-Heinmann; 2002.
[35] Sowerby R, Duncan JL. Failure in sheet metal in biaxial tension. Int J Mech Sci 1971;13:217–29.
[36] Yoshida K, Suzuki N. Forming limit stresses predicted by phenomenological plasticity theories with anisotropic work-hardening behavior. Int J Plasticity 2008;24:118–39.